# Title: *Admp* regulates tail bending by controlling the intercalation of the ventral epidermis through myosin phosphorylation.

Yuki S. Kogure [1], Hiromochi Muraoka [1], Wataru C. Koizumi [1], Raphaël Gelin-alessi [1], Benoit Godard [2], C. P. Heisenberg [2], Kotaro Oka [1,3,4] and Kohji Hotta [1]*

**Affiliations**

[1] Department of Biosciences and Informatics, Faculty of Science and Technology, Keio University, Kouhoku-ku, Yokohama 223-8522, Japan

[2] Institute of Science and Technology Austria, Klosterneuburg, Austria

[3] Waseda Research Institute for Science and Engineering, Waseda University, 2-2 Wakamatsucho, Shinjuku, Tokyo 162-8480, Japan

[4] Graduate Institute of Medicine, College of Medicine, Kaohsiung Medical University, Kaohsiung City 80708, Taiwan

*** Correspondence:** Kohji Hotta**,** khotta@bio.keio.ac.jp

**Running Title**: Polarity by *Admp* control tail bending

**Summary Statement**: *Admp* is an upstream regulator of the bending of the tail in the tailbud embryo regulating tissue polarity of the ventral midline epidermis by phosphorylation of myosin.

**Keywords:** tunicate, tail bending, intercalation, polarity, apical-constriction, cryptic lamellipodia

**Abstract:**

Chordate tailbud embryos have similar morphological features, including a bending tail. A recent study revealed that the actomyosin of the notochord changes the contractility and drive tail bending of the early *Ciona* tailbud embryo. Yet, the upstream regulator of tail bending remains unknown. In this study, we find that *Admp* regulates tail bending of *Ciona* mid-tailbud embryos. Anti-pSmad antibody signal was detected at the ventral midline tail epidermis. *Admp* knock-down embryo completely inhibited the ventral tail bending and reduced the number of the triangular-shaped cells, which has the apical accumulation of the myosin phosphorylation and inhibited specifically the cell-cell intercalation of the ventral epidermis. The degree of myosin phosphorylation of the ventral cells and tail bending were correlated. Finally, the laser cutter experiments demonstrated the myosin-phosphorylation-dependent tension of the ventral midline epidermis during tail bending. We conclude that *Admp* is an upstream regulator of the tail bending by controlling myosin phosphorylation and its localization of ventral epidermal cells. These data reveal a new aspect of the function of the Admp that might be evolutionarily conserved in bilaterian animals.

**(main text approx. 6805/7000 words)**

## Introduction

Although chordates have various shapes and sizes in the adult stage, they have similar shapes during their organogenesis period, called the phylotypic stage (Klaus., 1983). During the phylotypic stage, chordates pass through neurulation and subsequently reach the tailbud stage. At the chordate tailbud stage, the embryo tail elongates along the anterior-posterior (AP) axis, and most tailbud embryos become curved shape (Richardson et al., 1997), bending the tail.

The protochordata, ascidian *Ciona intestinalis* type A (*Ciona robusta*) embryo also shows tail bending ventrally (ventroflexion) in the early- to mid- tailbud stages, and then the bending relaxed and start to bend dorsally (dorsiflexion) in order, even if the egg envelope is removed (Hotta et al., 2007).

This means that *Ciona* tail bending occurs independently without external force (Hotta et al., 2007a; Lu et al., 2020). Although it has been shown that a longitudinal pushing force is exerted by each notochord cell (Sehring et al., 2014; Zhou et al., 2015) and the tail elongation has suggested that the notochord actively produces an AP elongating force (Miyamoto and Crowther, 1985; Sehring et al., 2014; Spemann, 1987; Ubisch, 1939), the mechanism of tail bending in the tailbud embryo has been unknown until a recent study by Lu et al. (2020). They investigated the internal molecular mechanism that enables *Ciona* to bend its tail of early tailbud and reported that the main factor of the tail bending during early tailbud stages (stage 18 to stage 20) is that the different contraction force by the actomyosin in between the ventral and the dorsal side of the notochord. However, it is unclear what the upstream regulators involved in tail bending and the morphogenetic mechanisms involved in bending after stage (st.) 20.

To identify the upstream regulator of tail bending and investigate the later tail bending mechanism after st. 20 in the *Ciona* tailbud embryos, we performed

knock-down experiments, a morphological analysis of tailbud embryo using three-dimensional (3D) imaging, inhibitor treatment, immunostaining, and laser cutting experiments. Here we show that Admp regulates intercellular intercalation and apical accumulation by phosphorylated myosin (pMLC) in ventral midline epidermal cells, converting it into the mechanical resistance in the AP direction required for proper tail bending in mid-tailbud stages.

## Results

### *Admp* MO suppressed ventral tail bending but not dorsal tail bending

In some previous studies, *Admp* knock-down by anti-sense morpholino (*Admp* MO) mutant embryos did not appear to have tail bending (Imai et al., 2006; Imai et al., 2012; Pasini et al., 2006). We focused on the *Admp* as a candidate for the upstream regulator of the tail bending.

To confirm our hypothesis, we first performed microinjection of the morpholino anti-sense oligo (MO) and observed the phenotype with the time-lapse movie (Fig.1A, Suppl. Mov. 1).

As a result, no bending to ventral (ventroflexion) was observed at the mid-tailbud stages of the *Admp* MO embryo; afterward, bending to dorsal (dorsiflexion) was observed similar to WT. When phenotypes of *Admp* MO embryos and WT at st. 22 (in which WT ventroflexion becomes maximum) were compared (Fig. 1B), the bending angle of the *Admp* MO embryos was significantly reduced to less than 40 degrees (Fig. 1C; N = 11/11). Therefore, it was suggested that *Admp* specifically regulates ventroflexion of the ascidian tailbud embryo.

Furthermore, BMP inhibitor dorsomorphin also shows the defect of no bending of tail at mid-tailbud stage (SupplFig. 1A), supporting the notion that the Admp/BMP pathway regulates tail bending.

The *Admp* gene is one of the BMP ligands, and in *Ciona*, it has been reported that the Admp/Bmp signal induces the differentiation of ventral peripheral neurons (Imai et al., 2012; Waki et al., 2015) and that *Msxb* is involved in the differentiation of epidermal neurons as a downstream of *Admp* (Imai et al., 2012). Next, we investigated whether the Admp-downstream target, *Msxb*, also regulates the tail bending. However, even if the *Msxb* has been knocked down, the ventroflexion seems to be normal (Suppl. Fig. 1B).

Therefore, we hypothesized that *Admp* might have another molecular pathway that controls the morphology of tail bending, apart from the downstream pathway of *Msxb* that controls the differentiation of ventral peripheral neurons (Roure and Darras, 2016; Waki et al., 2015).

Although a previous study has shown that notochord actomyosin asymmetry is responsible for tail bending (Lu et al., 2020), asymmetric localization of notochord actomyosin in the dorsoventral region was still observed even if in the *Admp*-knockdown embryo at st. 22 (Suppl. Fig. 2), suggesting that *Admp*'s inhibition of tail bending was due to factors other than notochord actomyosin asymmetrical localizations during st. 18 to st. 20.

**Smad phosphorylation in ventral midline epidermal cells**

In *Ciona*, *Admp* is expressed in the endoderm and lateral epidermis (Imai et al., 2012). Since *Admp* is a morphogen, it can act in a place far from the place of the expression. In vertebrate, *Admp* is expressed dorsally and moves to the opposite side to specify the ventral fate and it is difficult to expect the target place from its gene expression pattern. On the other hand, it was known that *Admp* promotes *bmp4* expression and controls the positioning of *bmp4* expression during regeneration of left-right asymmetric fragments in planarian (Gaviño and Reddien, 2011).

In *Ciona*, *Admp* expression appeared normal in *Bmp2/4* morphants but *Bmp2/4*

expression was suppressed in *Admp* morphants (Imai et al., 2012). The Bmp target, Smad was phosphorylated and the phosphorylated Smad translocates into the nucleus and activates the target genes (Blitz and Cho, 2009; De Robertis, 2009; Imai et al., 2012). The Smad signal of the ventral epidermal cells disappears in *Ciona* embryo injected with *Admp* MO at late gastrula stage (Waki et al., 2015).

To know when and where the Admp/BMP signal was transmitted, we performed the antibody staining of phosphorylated Smad, pSmad1/5/8 (Fig. 1D). As a result, supporting the previous study (Waki et al., 2015), pSmad signal was observed at the ventral midline epidermal cells after the late gastrula stage (Fig. 1D), and no specific signal was detected at the dorsal side from gastrula to the initial tailbud period. From these results, it was shown that Admp / BMP signal was transmitted to ventral midline epidermal cells.

**The phenotype of *Admp MO* embryos decreased triangular-shaped cells.**

Next, we investigated the phenotype of *Admp* MO embryo at single-cell level especially focusing on the ventral midline epidermal cells that undergo Smad phosphorylation. The median section image of the tailbud embryo at st. 22 was analyzed (Fig. 2A). Tail tissues consisting of the muscles, notochord, endoderm strand, and neural tubes were anatomically observed in WT embryos and *Admp* MO embryos. However, focusing on the shape of ventral epidermal cells, “triangular” cells with the apex on the apical side (Fig. 2A squares, enlarged in Fig. 2B) were preferentially observed in WT embryos than MO embryos (Fig. 2C).

**Admp controls the apico-basal localization of pMLC in the ventral epidermal cells**

Both the accumulation of F-actin and pMLC were observed on the apical side of the triangular cells (Fig. 2D arrowheads). On the other hand, the asymmetric localization of phosphorylated myosin between the apical surface and the basal plane was reduced in *Admp* MO embryo (Fig. 2E). This result suggests that *Admp* MO inhibited the relocation of pMLC and kept it on the basal plane.

Supporting this, there was a correlation between the extent of apical phosphorylation of the ventral epidermis and local tail bending angle (Suppl. Fig. 3) in WT embryo, and the tail bending was inhibited by Y27632 treatment (Suppl. Fig. 4).

**The tension of ventral epidermal cells causes tail bending**

From these results, it was considered that Admp controls the localization of pMLC to the apical side on the ventral epidermal cells that promote tail bending. Then, does the localization of pMLC on the apical side generate the force of tail bending?

To verify whether the localization of phosphorylated myosin of apical accumulation in epidermal cells causes tension of tail bending, the apical surface of the ventral or dorsal epidermal cells was cut (Fig.3, yellow lines) with a laser cutter. The orientation of the cuts was along with medio-lateral (ML) axis.

As a result, the relaxation did not occur when the dorsal midline epidermal cells were cut, but the ventral midline epidermal cells show the relaxation to the dorsal side, indicating the tension along with the AP axis at the ventral midline epidermal cells (Fig. 3A and 3B, Suppl. Mov. 2). In addition, no relaxation was observed when the cutting of both ventral and dorsal sides in Y27632-treated embryos (Fig. 3C and 3D). We further investigated whether the ventral relaxation

depend on the orientation of the cuts with AP axis vs ML axis in ventral midline cells. As a result, the cut by AP orientation has no significant relaxation in the tail bending (data not shown).

These results indicated that phosphorylated myosin caused tension in the ventral midline epidermis enabling ventroflexion at st. 22.

**Triangular cells are epidermal cells undergoing intercalation at the ventral midline during tail bending**

We investigated how the triangular cells contribute to the tail bending. The median cross-section image at the tailbud stage indicated that the phosphorylated myosin emerged the anterior-posterior border from st. 21 (Fig. 4, st. 21 arrowheads), accumulates apical side and makes triangular cells at st.22 (Fig. 4, st. 22 arrowheads), decreased the number accompanying with the cell shape becoming trapezoid after st. 23 (Fig. 4, st. 23; Suppl. Fig. 4), and finally disappeared at st. 24.

The ventral view of the anti-pMLC stained embryo showed that ventral midline cells, including triangular cells, were undergoing cell-cell intercalation (Suppl. Fig. 4Ab-Hb') and eventually formed a row of median epidermal cells (Fig. 4B; Suppl. Fig. 4Ab-Hb').

The 3D reconstructed image of the intercalating cell (Suppl. Fig. 5) revealed that these cells have intrusion relatively larger area in the basal plane (Suppl. Fig. 5C and 5D, orange areas) than the apical side (Suppl. Fig. 5C and 5D, red areas) that makes a triangular shape on the median cross-section (Fig. 4B). This special shape of the intercalating cells is thought to contribute to the bending shape of the epidermal tissue (Fig. 4B, st. 21-23).

At st. 24, the WT *Ciona* tail epidermis finally forms eight distinct single-cell rows after cell-cell intercalation (Fig. 4C) (Hotta et al., 2007; Pasini et al., 2006). The

eight rows, consisting of three rows of dorsal, two rows of lateral, and three rows of dorsal epidermal cells, are aligned (Fig. 4C a-c').

On the other hand, a 3D reconstructed image of the *Admp* MO embryo has shown a specific failure of the ventral three-rows' intercalation (Fig. 4C e-e').

Dorsomorphin treatment also shows a similar ventral midline intercalation defect at ventral epidermal cells (Suppl. Fig. 6).

These results indicate that *Admp* regulates ventral epidermal cell-cell intercalation. These intercalating cells are suggested to invade from the basal plane side and mediate tail bending by forming a triangular shape in the median cross-section (Fig. 4A and 4B).

## Discussion

### Admp is an upstream regulator of the tail bending

In this study, we found that *Admp* regulate the localization of the myosin phosphorylation (Fig. 2) and the cell-cell intercalation at the ventral epidermis (Fig. 4). How the intercalation of ventral midline cells functions in tail bending? The ventral epidermis undergoing intercalation would relatively slow elongation during st. 20 to st. 22 than the already intercalated dorsal epidermis (Suppl. Fig. 7). Considering the notochord as the main force of elongation (Dong et al., 2011; Hara et al., 2013; Lu et al., 2019), ventral epidermal cells might resist against the AP elongation force of notochord during st. 20 to st. 22 and generate tension temporally in the ventral midline epidermal cells (Fig. 3). Supporting with this, the ventral midline epidermis did not change the AP length in the beginning of the intercalation (Suppl.Fig. 8A). The apically accumulated pMLC during intercalation (Fig. 4B) may contribute to the halt of the AP elongation of the apical side of the triangular cells like a hinge (Suppl.Fig. 8B, red arrows) of adjacent cells during tail bending (Suppl.Fig. 8B, orange). On the contrary, the

basal plane of these cells can allow elongation with AP direction. By controlling such intercalation of the ventral epidermal cells through myosin phosphorylation, Admp might finally induce the ventroflexion (Fig. 1).

Originally, the Admp/BMP pathway plays a central role in establishing, maintaining, and regenerating the DV axis among bilaterian animals (Gaviño and Reddien, 2011). In the ascidian, both gain- and loss-of-function experiments demonstrate that *Admp* expressed in the B-line medial vegetal cells acts as an endogenous inducer of the ventral epidermis midline (Pasini et al., 2006). *Admp* is required for sensory neuron differentiation of the ventral epidermis via the *Tbx2/3* and *Msxb* genes (Waki et al., 2015). The no tail-bending phenotype of the *Msxb* MO (Suppl. Fig. 1B) indicates the tail bending was not regulated by *Msxb* but regulated as a downstream pathway of *Admp*.

How does Admp/BMP signaling to regulate the polarity of the ventral epidermis via myosin phosphorylation? Several studies support this pathway. In other animals, the Admp/Bmp regulatory pathway is related to the maintenance and/or regeneration of DV polarity (Chang et al., 2016; Gaviño and Reddien, 2011). In this study, it was indicated that the localization of the pMLC was translocated from the basal side (dorsal side) to the apical side (ventral side), which changes the cell polarity during early to mid-tailbud stages (Fig. 4A). This might be because of DV polarity change at the cellular level by Admp/Bmp regulatory pathway.

Recent studies show that SMAD3 drives cell intercalation underlies secondary neural tube formation in the mouse embryo (Gonzalez-Gobartt et al., 2021). Moreover, it was known that the BMP-Rho-ROCK1 pathway targets MLC to control actin remodeling in fibroblasts (Konstantinidis et al., 2011).

This pathway regulates fibroblast migration without affecting cell proliferation. Supporting this, our preliminary data show *Admp*-MO did not affect the cell number consisting of ventral midline epidermis but changed cell number of the dorsal epidermis, which is thought to be out of the Admp regulation (Fig. 1D). The DV differential epidermis proliferation was considered a passive response to mechanical forces (Lu et al., 2020).

**Model of ascidian tail bending**

From our findings, *Admp* controls ventral bending of the tail during tailbud embryo stages. The proposed model (Fig. 5) is that Admp phosphorylates Smad in the ventral epidermis, and pSmad controls the cell-cell intercalation in the ventral epidermis by controlling their localization pMLC that finally generate tension in the ventral epidermis causing tail bending (Fig. 5).

The intercalating cells have protrusions in the bilateral side of the basal domain, which resembles the cryptic lamellipodium reported in Caco2 cultured cells (Ozawa et al., 2020).

We propose that the pMLC was involved in the cell intercalation and accumulated apical of ventral midline epidermal cells during st. 21–23 (Fig.4D-F), but that it also confers a resistance along the AP axis (Fig. 5, blue arrows) against notochord elongation force (Fig. 5, orange arrow).

So, the tissue responsible for tail bending in *Ciona* might be changed with developmental stages: phase I is notochord generating asymmetric contraction force before st. 20 as (Lu et al., 2020) and phase II is ventral epidermis undergoing intercalation after st. 20 (Suppl. Fig. 4; Suppl. Fig. 7).

Because during st. 21 to 24, the notochord changes the cell shape using circumferential contraction force (Lu et al., 2019; Mizotani et al., 2018; Sehring et al., 2014). The transverse loading generated by the circumferential constrictive

force on a compression-resisting system is converted into a pushing force that is especially higher along the longitudinal axis (Lu et al., 2019; Miyamoto & Crowther, 1985). Supporting this, our laser cutting experiments revealed the presence of stress at the ventral midline epidermal cells at st. 22 (Fig. 3). Y27632-treated embryos did not show any ventral tail bending during st. 22, which also supports this model (Fig. 5).

**The evolutionary role of *Admp***

We conclude that *Admp* regulates ventroflexion during mid-tailbud stages (st. 20 to st. 23) by the myosin-dependent force resistance in a small population of intercalating ventral midline epidermal cells against AP elongation force by the notochord. Our study provides insight into understanding the molecular and mechanical background that contributes to the conserved shape of the chordate embryo during the organogenesis period. Many studies have not so far focused on the bending of the tailbud embryo; there seemed to be many defects of tail bending in chordate embryos when ADMP/BMP was knocked down [zebrafish: (Esterberg et al., 2008; Willot et al., 2002); frog: (Dosch and Niehrs, 2000; Kumano et al., 2006)].

To confirm the embryo morphological function of *ADMP* throughout cell polarity found in this study evolutionarily conserved among animals, the morphogenetic roles of ADMP in other animals should be investigated in a future study.

**Materials and methods**

**Ascidian samples**

*C. robusta* (*C. intestinalis* type A) adults were obtained from Maizuru Fisheries Research Station (Kyoto University, Kyoto, Japan), Onagawa Field Center (Tohoku University, Sendai, Japan), and Misaki Marine Biological Station (University of Tokyo, Tokyo, Japan) through the National Bio-Resource Project

(NBRP; Japan) and from the Roscof Marine Station (Roscof, France). Eggs were collected by dissection of the gonoducts. After artificial insemination, fertilized eggs were incubated at 20°C until fixation or observation. Developmental stages were followed Hotta's stages (Hotta et al., 2007a; Hotta et al., 2020). In inhibiting phosphorylation of 1P myosin, Y27632 (nacalai tesque) was applied to embryos at 10 μM after 7 hpf (late neurula, st. 16). Dorsomorphin (Sigma-Aldrich) was applied to embryos at 10 μM after 7 hpf (late neurula, st. 16).

**Immunostaining and quantifying pMLC intensity**

To detect activation of the Admp/BMP signaling pathway, we followed the same method described previously (Waki et al., 2015). The signal was visualized with a TSA kit (Invitrogen) using horseradish peroxidase-conjugated goat anti-rabbit immunoglobulin-G and Alexa Fluor 488 tyramide.

The method of pMLC antibody staining was as follows. Embryos were fixed in 3.7% formaldehyde in seawater for 30 min and then rinsed with phosphate-buffered saline with Tween (PBST; 0.2% Triton-X in PBS) for 3 h. Embryos were incubated in PBST containing 10% goat serum for 3 h at room temperature or overnight at 4°C. Primary antibody (anti-rabbit Ser19 phosphorylated-1P-myosin, Cell Signaling, USA) was diluted 1:50 then incubated for 3 h at room temperature or overnight at 4°C. The primary antibody was washed with PBST for 3 h. A poly-horseradish peroxidase (HRP) secondary antibody (goat anti-rabbit IgG, Alexa Fluor 488 Tyramide SuperBoost Kit, USA) was applied for 3 h and washed in PBST for 3 h. Alexa Fluor dye tyramide (Alexa Fluor 488 Tyramide SuperBoost Kit) was added to the reaction buffer for 5 to 8 min to induce a chemical HRP reaction. Embryos were dehydrated through an isopropanol series and finally cleared using a 2:1 mixture of benzyl benzoate and benzyl alcohol.

pMLC accumulation was quantified by measuring the intensity along the ventral tail epidermis using Fiji image analysis software. The signal in the brain region

was taken as the positive control because its signal was detected even in Y27632 treated-embryos, indicating RhoA kinase (ROCK)-independent expression. The relative intensity of pMLC normalized to the intensity of the brain region in each individual was calculated by ImageJ for the comparative analysis among different individuals.

**Laser-cutter experiment**

The UV laser cutter setup is based on a previous description (Behrndt et al., 2012). The laser cutter was equipped with a Zeiss 63x 1.2 NA water immersion lens for viewing FM4-64 (ThermoFisher) stained *Ciona* embryos. Laser cutting in the tail epidermal cells was performed during the tailbud period by applying 25 pulses of straight 355 nm laser lines at 20 mW and an intensity of 0.7 to the lateral boundary between midline epidermal cells. Fluorescent images of FM4-64 were acquired concurrently at 488 nm excitation. Epidermal cells are a mono-layer, and we cut each AP junction (Fig. 3). All cutting experiments were performed at a constant temperature of 18°C using a custom-built cooling stage. Relaxation measured the area of movement of the tail region 3 s after laser cutting.

**Gene knock-down**

The MOs (Gene Tools, LLC) against *Msxb* and *Admp*, which block translation, were designed according to the previous study (Imai et al., 2006; Waki et al., 2015); *Admp*, 50-TATCGTGTAGT TTGCTTTCTATATA-30; *Msxb*, 50 – ATTCGTTTACTGTCATTTTTAATTT - 30. These MOs at 0.25 to 0.50 mM were injected into an unfertilized egg and incubated until observation. To know the phenotype of *Admp* MO embryo at the single-cell level, embryos were stained by Alexa 546 phalloidin (Thermo Fisher).

**Acknowledgments**

*Ciona intestinalis* adults were provided by Dr. Yutaka Satou (Kyoto University) and Dr. Manabu Yoshida (the University of Tokyo) with support from the National Bio-Resource Project of AMED, Japan. We thank Dr. Hidehiko Hashimoto and Mr. Yuji Mizotani for technical information with 1P-myosin antibody staining.

We thank Dr. Yutaka Sato for the valuable discussion of *Admp* and for sharing unpublished RNA-seq data. We thank Ms. Maki Kogure for the construction of the 3DCAD of the intercalating epidermal cell.

**Competing interests**

The authors declare no competing or financial interests.

**Author contributions**

Y.S.K., H.M., W.C.K, and K.H. designed and performed research. Y.S.K. , W.C.K, R.G. and H.M. analyzed data. W.C.K., B.G., and K.H. performed the laser cutter experiments. H.M. performed 1P-myosin analysis. Y.S.K. and K.H. wrote the manuscript. K.O. and C.P.H critically revised the manuscript. K.H. and K.O. supervised research.

**Funding**

This work was supported by JSPS KAKENHI, Grant Numbers JP16H01451, JP16K07426 and 21H00440.

## Data availability

All data generated or analyzed during this study are included in the manuscript and supporting files.

## Figure legends

**Fig. 1.** *Admp* affects the tail bending of early tailbud stage embryo, and pSmad was detected at ventral midline epidermis.

(A) Time-lapse movie of WT and *Admp* MO embryo. WT and *Admp* MO embryos were developed in the same dish, and WT embryos were stained by NileBlue B to distinguish. Note that *Admp* MO suppressed ventral tail bending (”ventroflexion”) during early to mid taibud stages (red double-headed arrow) but not dorsal tail bending (“dorsiflexion”) during the late tailbud stage (orange double-headed arrow) after “relaxation”( blue double-headed arrow) at the beginning of late tailbud stage. The developmental stage and time after fertilization was shown in each picture of WT. Scale bar = 100 μm. A: anterior, P: posterior, D: dorsal, V: ventral. (B) The definition of the bending angle. The bending angle of the embryo tail was defined as the intersection angle of the straight line perpendicular to the neural tube of the trunk and the anterior-posterior border of the notochord cell, which is the 20 th from the anterior side. (C) Quantification of bending angle θ of WT(n=8) and *Admp* MO (n=10) embryo. The bending angle was significantly reduced in *Admp* MO embryo. (D) An antibody staining against phosphorylated Smad1/5/8 (green). The Admp / BMP signals were detected from the late gastrula at ventral midline cells (parenthesis). Scale bar = 50 μm.

**Fig. 2. Comparison of the phenotype of Admp MO with WT embryo.**

(A) Midline section view of WT tailbud embryo and *Admp* MO embryo at st. 22 by staining of F-actin. Arrowheads indicate the position of the triangular-shaped

cells. The regions in both yellow and green rectangles are enlarged in (B). Abbreviations: noto, notochord; nt, neural tube; es, endodermal strand.

(B) Triangular cell (yellow rectangular) and non-triangular cell (green rectangular) of WT embryo. Each cell shape was traced (red dotted lines) in lower panels. The triangular cells were defined as triangle-shaped cells with the apex on the apical side.

(C) The ratio of the number of triangular cells and the number of midline cells. It has been reported the driving forces of the tail bending originate in the anterior part of the tail (Lu et al., 2020). Therefore, we counted the number of triangular cells in the anterior part of the tail. Triangular cells were significantly reduced MO embryos. (D) Double staining of F-actin and phosphorylated myosin light chain (pMLC) of the ventral midline of WT and *Admp* MO embryo at st. 22. Both F-actin and pMLC accumulated at the apical side of triangular cells (arrowheads). The localization of pMLC on the basal side of the epidermis seemed to be weak in WT but strong in *Admp* MO. (E) Relative pMLC intensity ratio between the apical and basal side of the epidermis in WT (N = 10) and *Admp* MO (N = 7). Asterisk indicates statistically significant (t-test, *: $p< 0.05$, **: $p<0.01$). The error bar indicates S.D.

**Fig. 3. Laser-cut experiment for the AP cell-cell border of the tail epidermis.**
(A) Laser-cutting of the dorsal and ventral midline epidermis of the wild type at st. 22. Epidermal cells are a monolayer. In the laser cut experiment, we cut each AP junction (yellow lines). (B) Movement of the area before and after the laser cut was calculated as relaxation (N = 5).

(C) Laser-cutting of the dorsal and ventral midline epidermis of Y27632-treated embryo at st. 22 (N = 5). In the laser cut experiment, we cut each AP junction (yellow lines). (D) The relaxation in the case of ventral cut between WT and

Y27632 embryo was compared. The ventral cut in the Y27632-treated embryo did not show relaxation.

Asterisk indicates statistically significant (t-test, *: $p < 0.05$). The error bar indicates S.D.

**Fig. 4. Change of the distribution of pMLC and the cell-cell intercalation of epidermal cells during the tailbud period.**

(A) Left column is the antibody staining of 1-phosphorylated-myosin (pMLC) from st. 20 to 24 in wild type (WT). The Middle column is the enlarged view of the dotted rectangle in each stage. Arrowheads show pMLC accumulation in the apical domain of the ventral midline epidermal cells. Scale bar = 50 μm. The right column shows the schematic drawing of the distribution of pMLC (shown in red). In st. 20, pMLC localized the basal side of the epidermis. In st. 21, pMLC has appeared at the AP cell border. At st. 22, the pMLC accumulated at the apex of the apical domain and the cell shape changed into triangular (orange-colored cell). The pMLC localization at the basal side was reduced. At st. 23, the apex of the apical domain becomes broader. At. st. 24, the pMLC accumulation of both apical and basal sides disappears. (B) Schematic drawing of the cell-cell intercalation of the ventral midline epidermal cells. Orange-colored cells start to intercalate at st. 20. During st. 21-23, the orange cell changes the shape into the “iron” shape shown in Suppl. Fig. 5. The orange cell start intrusion from basolateral sides with pMLC protrusions (red-colored). As the ventral midline epidermis consists of orange cells with a smaller apical domain area than the basal domain, the overall tissue becomes bending (blue arrow). The midline section image of the orange cell shows the triangular shape. At st. 24, the cell-cell intercalation was completed, and the orange cell align on the midline. The 3D models were generated by FUSION 360 educational ver. (Autodesk). (C) The alignment of the tail epidermal cells of WT and *Admp* MO embryo at st. 24. When the cell-cell intercalation has

finished in WT at st. 24 (a – c'), the tail epidermal cells consist of 8 rows: dorsal (yellow), two dorsal medio-lateral (green), ventral (red), two ventral medio-lateral (orange) and two lateral (blue) rows. On the other hand, there is a specific inhibition of the intercalation of the ventral side in *Admp* MO embryo (e – e'). (N = 4 in WT and 4 in *Admp* MO)

**Fig. 5. Model of embryonic tail bending in *Ciona*.**

The previous study reported that the asymmetric actomyosin contraction in the notochord is the main factor for the tail bending until st. 20 (upper blue rectangular). On the other hand, Admp/BMP signaling (the flow by red rectangles) transmits the signal to the ventral midline epidermal cells as phosphorylated Smad from neurula to initial tailbud. pSmad translocates the localization of the pMLC from the basal side (dorsal side) to the apical side (ventral side), which changes the cell polarity and promotes the cell-cell intercalation of the ventral midline epidermal cells during early to mid-tailbud stages (st. 20 to st. 23). The ongoing mediolateral intercalation at the ventral epidermis confers a resistance (orange arrows) to AP elongation force (blue arrow) that is possibly provided by the notochord, which causes the bending tail shape in the *Ciona* tailbud embryo at st. 22. On the other hand, the *Admp* MO or dorsomorphin-treatment disrupts the cell polarity and causes the no tail-bending embryo at st. 20-23 and incomplete intercalation at st. 24 (the flow by green rectangles). Inhibition of pMLC by Y27632 also causes no ventral bending. Final overall embryo shape at st. 24 is similar among WT and *Admp* MO embryos, but the ventral cell-cell intercalation was disrupted. Thus, Admp/BMP signaling, apart from its role of peripheral nervous system (PNS) differentiation (lower blue rectangular), regulate temporal tail bending during early to middle tailbud stages (st. 20 to st. 23).

**Suppl. Mov. 1. Time-lapse movie of WT (left) and *Admp* MO (right) embryo from late neurula stage 16 to late tailbud stage 25**

Both embryos are incubated in the same dish. The WT embryo was stained by NileBlue B (Matsumura et al., 2020). Depending on the tail morphology, the movie flame was surrounded by different colors. red: ventroflexion, blue: relaxation of ventroflexion, orange: dorsiflexion.

**Suppl. Mov. 2. Laser cutting experiment of the midline tail epidermis**

The dorsal (left) and ventral (right) midline epidermal AP cell borders of the WT mid-tailed embryos were cut with a laser cutter. The arrowheads indicate the cutting point by the laser cutter. The angle of the ventroflexion was relaxed when cut on the ventral side but not on the dorsal side, indicating the AP tension of the ventral midline epidermis (N = 3 each).

**Suppl. Fig. 1. Morphants of tail bending.**

(A) mid-tailbud stage embryo of WT, DMSO treatment, and Dorsomorphin. DMSO and Dorsomorphin were treated after the mid neurula stage (st. 15). The dorsomorphin-treated embryo didn't bend tail, similar to the *Admp* MO embryo (Fig.1A).

(B) MOs against *Msxb* were injected. While *Admp* MO was affected the tail bending (Fig.1A), *Msxb* MO was not affected the tail bending. Scale bar, 100 μm. The number of examined embryos and the proportion of representative embryos are shown in each panel, respectively. All embryos are shown anterior to the left.

**Suppl. Fig. 2. the existence of ventrally localized actomyosin in the notochord during embryonic tail bending at st. 22.**

(A) F-actin localization of notochord in both WT and *Admp* MO was measured on the yellow lines across dorso-ventral (DV) axis.

(B) The intensity ratio between ventral and dorsal F-actin. If the intensity of the ventral side (red arrow in A) is stronger than the dorsal side (orange arrow in A), the ratio becomes more than 1. In *Admp* MO embryos, F-actin is significantly localized ventrally (WT, N=8; *Admp* MO, N=10). Asterisk indicates statistically significant (t-test, *: $p< 0.05$). The error bar indicates S.D.

**Suppl. Fig. 3. Local tail bending and relationship with pMLC**

(A) Local curvature at st. 22 and AP axis in wild type (blue dots) and Y27632-treated (orange dots) embryos. To investigate local tail bending, we quantified the local tail curvature along the tail midline. The 40 plots were assigned to the midline of the tail region. We selected three points (plots 1, 6, and 11) that were chosen every five points, alternating from posterior to anterior along the tail midline (points i, i+5, and i+10 [i=1, 2…30]). The circumscribed circle was defined by these three points. The Local C.I. was calculated as follows: $1/R \times L$, where $1/R$ is the local tail curvature and L is the tail length. Thus, 30 values of Local C.I. along with the AP axis were defined.

(B) pMLC intensity on the ventral midline along with the AP axis. Different colors indicate a different individual (N=5). pMLC accumulation was quantified by measuring the intensity and the ventral tail epidermis from points 5 to 35 using Fiji image analysis software.

(C) Correlation between local pMLC intensity and the local curvature in WT embryo.

**Suppl. Fig. 4. pMLC antibody staining during tailbud period.**

(Aa–Hc') Antibody staining of pMLC from st. 18 to st. 24 in wild type (rows A to G) and st. 22 in Y27632-treated (row H) embryos. Arrowheads show pMLC accumulation in the ventral midline epidermal cells. The part surrounded by the dotted square is enlarged to the panel on the right. Brackets indicate the range of the midline epidermal region. The midline epidermal cells are intercalated, and the region becomes narrower (see Suppl. Fig. 7). Scale bar = 20 μm.

**Suppl. Fig. 5 Three-dimensional reconstruction of ventral midline epidermal cells during tail bending.**

(A) Stack images of ventral epidermal cells at st. 22 was traced by using an anti-pMLC antibody staining embryo.

(B) A single epidermal cell was modeled by using Avizo6 software. Different color corresponds to the same-colored cell in (A).

(C) Representative morphology of ventral midline cells. The apical area is surrounded by red dots line, and a yellow dots line surrounds the basal area. Note that the apical area is smaller than the basal area. The cell is bipolar and has protrusions from basal parts.

(D) The 3D model that reflects the shape of ventral epidermal cells in (C). The 3D tissue model used in st. 21-23 in Figure 4 is composed of 10 of these 3D model cells.

**Suppl. Fig. 6. The alignment of the tail epidermal cells of DMSO-treated and Dorsomorphin-treated embryo at st. 24.**

The cell-cell intercalation was completed in the DMSO-treated embryo (left), and the tail epidermal cells consist of 8 rows: dorsal (yellow), two dorsal medio-lateral (green), ventral (red), two ventral medio-lateral (orange) and two laterals (blue) rows. On the other hand, there is a specific inhibition of the intercalation of the ventral row in Dorsomorphin-treated embryos (right). (N = 2 in DMSO and 2 in Dorsomorphin)

**Suppl. Fig. 7. The alignment of the tail midline epidermal cells during the tailbud period.**

From 3D reconstructed confocal stack images by F-actin staining of tailbud embryos (st.18 in A, st.19 in B, st.20 in C, st. 21 in D, st. 22 in E, st. 23 in F and st. 24 in G), cell shapes of both dorsal and ventral midline epidermal cells are traced (yellow lines). Note that cell-cell intercalation completes earlier on the dorsal midline than on the ventral midline.

**Suppl. Fig. 8. The difference between ventral and dorsal outline length.**

(A) Time course of dorsal outline length (red line) and ventral outline length (blue line) of the tail region. Each dotted line indicates the corresponding developmental *Ciona* stage.

(B) The schematic model of the halt of the AP elongation during tail bending by the apically accumulated pMLC. Before the intercalation, midline cells only consist of beige cells (st. 19). During intercalation of ventral epidermal cells, medio-lateral cells (orange) intrude to the midline cells (beige) from basal plane. The apically accumulated pMLC (red) may contribute to the halt of the elongation of the apical side of the triangular cells like a hinge (red arrows) of adjacent cells

but the basal plane of orange cells can allow elongation during ventroflexion (st. 20 to st. 21). During relaxation, the intercalation is finishing. The apical accumulation of pMLC decrease and recover the apical elongation of epidermal cells (st. 22 to st. 24).

## References

**Behrndt, M., Salbreux, G., Campinho, P., Hauschild, R., Oswald, F., Roensch, J., Grill, S. W. and Heisenberg, C.-P.** (2012). Forces driving epithelial spreading in zebrafish gastrulation. *Science* **338**, 257–60.

**Blitz, I. L. and Cho, K. W. Y.** (2009). Finding partners: How BMPs select their targets. *Dev. Dyn.* **238**, 1321–1331.

**Chang, Y.-C., Pai, C.-Y., Chen, Y.-C., Ting, H.-C., Martinez, P., Telford, M. J., Yu, J.-K. and Su, Y.-H.** (2016). Regulatory circuit rewiring and functional divergence of the duplicate admp genes in dorsoventral axial patterning. *Dev. Biol.* **410**, 108–18.

**De Robertis, E. M.** (2009). Spemann's organizer and the self-regulation of embryonic fields. *Mech. Dev.* **126**, 925–941.

**Dong, B., Deng, W. and di Jiang** (2011). Distinct cytoskeleton populations and extensive crosstalk control Ciona notochord tubulogenesis. *Development* **138**, 1631–1641.

**Dosch, R. and Niehrs, C.** (2000). Requirement for anti-dorsalizing morphogenetic protein in organizer patterning. *Mech. Dev.* **90**, 195–203.

**Esterberg, R., Delalande, J.-M. and Fritz, A.** (2008). Tailbud-derived Bmp4 drives proliferation and inhibits maturation of zebrafish chordamesoderm. *Development* **135**, 3891–3901.

**Gaviño, M. A. and Reddien, P. W.** (2011). A Bmp/Admp Regulatory Circuit Controls Maintenance and Regeneration of Dorsal-Ventral Polarity in Planarians. *Curr. Biol.* **21**, 294–299.

**Gonzalez-Gobartt, E., Blanco-Ameijeiras, J., Usieto, S., Allio, G., Benazeraf, B. and Martí, E.** (2021). Cell intercalation driven by SMAD3 underlies secondary neural tube formation. *Dev. Cell* **56**, 1147-1163.e6.

**Hara, Y., Nagayama, K., Yamamoto, T. S., Matsumoto, T., Suzuki, M. and Ueno, N.** (2013). Directional migration of leading-edge mesoderm generates physical forces: Implication in Xenopus notochord formation during gastrulation. *Dev. Biol.* **382**, 482–495.

**Hotta, K., Mitsuhara, K., Takahashi, H., Inaba, K., Oka, K., Gojobori, T. and Ikeo, K.** (2007a). A web-based interactive developmental table for the Ascidian Ciona intestinalis, including 3D real-image embryo reconstructions: I. From fertilized egg to hatching larva. *Dev. Dyn.* **236**, 1790–1805.

**Hotta, K., Yamada, S., Ueno, N., Satoh, N. and Takahashi, H.** (2007b). Brachyury-downstream notochord genes and convergent extension in Ciona intestinalis embryos. *Dev. Growth Differ.* **49**, 373–382.

**Hotta, K., Dauga, D. and Manni, L.** (2020). The ontology of the anatomy and development of the solitary ascidian Ciona: the swimming larva and its metamorphosis. *Sci. Rep.* **10**, 1–16.

**Imai, K. S., Levine, M., Satoh, N. and Satou, Y.** (2006). Regulatory Blueprint for a Chordate Embryo. *Science (80-. ).* **312**, 1183–1187.

**Imai, K. S., Daido, Y., Kusakabe, T. G. and Satou, Y.** (2012). Cis-acting transcriptional repression establishes a sharp boundary in chordate embryos. *Science (80-. ).* **337**, 964–967.

**Klaus., S.** (1983). *The evolution of patterning mechanisms: gleanings from insect embryogenesis and spermatogenesis.* (ed. GoodwinBC, HolderN, W.) Cambridge University Press.

**Konstantinidis, G., Moustakas, A. and Stournaras, C.** (2011). Regulation of Myosin Light Chain Function by BMP Signaling Controls Actin Cytoskeleton Remodeling. *Cell. Physiol. Biochem.* **28**, 1031–1044.

**Kumano, G., Ezal, C. and Smith, W. C.** (2006). ADMP2 is essential for primitive blood and heart development in Xenopus. *Dev. Biol.* **299**, 411–423.

**Lu, Q., Bhattachan, P. and Dong, B.** (2019). Ascidian notochord elongation. *Dev. Biol.* **448**, 147–153.

**Lu, Q., Gao, Y., Fu, Y., Peng, H., Shi, W., Li, B., Lv, Z., Feng, X.-Q. and Dong, B.** (2020). Ciona embryonic tail bending is driven by asymmetrical notochord contractility and coordinated by epithelial proliferation. *Development* **147**, dev185868.

**Matsumura, K. D., Nakamura, M. J., Koizumi, W. C., Hotta, K. and Oka, K.** (2020). Different strategies for tissue scaling in dwarf tailbud embryos revealed by single-cell analysis. *Dev. Biol.* **460**, 215–223.

**Miyamoto, D. M. and Crowther, R. J.** (1985). Formation of the notochord in living ascidian embryos. *J. Embryol. Exp. Morphol.* **86**, 1–17.

**Mizotani, Y., Suzuki, M., Hotta, K., Watanabe, H., Shiba, K., Inaba, K., Tashiro, E., Oka, K. and Imoto, M.** (2018). 14-3-3Ea Directs the Pulsatile Transport of Basal Factors Toward the Apical Domain for Lumen Growth in Tubulogenesis. *Proc. Natl. Acad. Sci.* 201808756.

**Ohtsuka, Y., Matsumoto, J., Katsuyama, Y. and Okamura, Y.** (2014). Nodal signaling regulates specification of ascidian peripheral neurons through control of the BMP signal. *Development* **141**, 3889–3899.

**Ozawa, M., Hiver, S., Yamamoto, T., Shibata, T., Upadhyayula, S., Mimori-Kiyosue, Y. and Takeichi, M.** (2020). Adherens junction regulates cryptic lamellipodia formation for epithelial cell migration. *J. Cell Biol.* **219**,.

**Pasini, A., Amiel, A., Rothbächer, U., Roure, A., Lemaire, P. and Darras, S.** (2006). Formation of the Ascidian Epidermal Sensory Neurons: Insights into the Origin of the Chordate Peripheral Nervous System. *PLoS Biol.* **4**, e225.

**Richardson, M. K., Hanken, J., Gooneratne, M. L. J., Pieau, C., Raynaud, a, Selwood, L. and Wright, G. M.** (1997). There is no highly conserved embryonic stage in the vertebrates: implications for current theories of evolutions and development. *Anat. Embryol.* **196**, 91–106.

**Roure, A. and Darras, S.** (2016). Msxb is a core component of the genetic circuitry specifying the dorsal and ventral neurogenic midlines in the ascidian embryo. *Dev. Biol.* **409**, 277–287.

**Sehring, I. M., Dong, B., Denker, E., Bhattachan, P., Deng, W., Mathiesen, B. T. and Jiang, D.** (2014). An Equatorial Contractile Mechanism Drives Cell Elongation but not Cell Division. *PLoS Biol.* **12**, e1001781.

**Spemann, H.** (1987). Embryonic Induction. *Am. Zool.* **27**, 575–579.

**Ubisch, V. L. v.** (1939). KEIMBLATTCHIMÄRENFORSCHUNG AN SEEIGELLARVEN. *Biol. Rev.* **14**, 88–103.

**Waki, K., Imai, K. S. and Satou, Y.** (2015). Genetic pathways for differentiation of the peripheral nervous system in ascidians. *Nat. Commun.* **6**, 8719.

**Willot, V., Mathieu, J., Lu, Y., Schmid, B., Sidi, S., Yan, Y. L., Postlethwait, J. H. H., Mullins, M., Rosa, F., Peyriéras, N., et al.** (2002). Cooperative action of ADMP- and BMP-mediated pathways in regulating cell fates in the zebrafish gastrula. *Dev. Biol.* **241**, 59–78.

**Zhou, J., Pal, S., Maiti, S. and Davidson, L. A.** (2015). Force production and mechanical accommodation during convergent extension. *Development* **142**, 692–701.

A

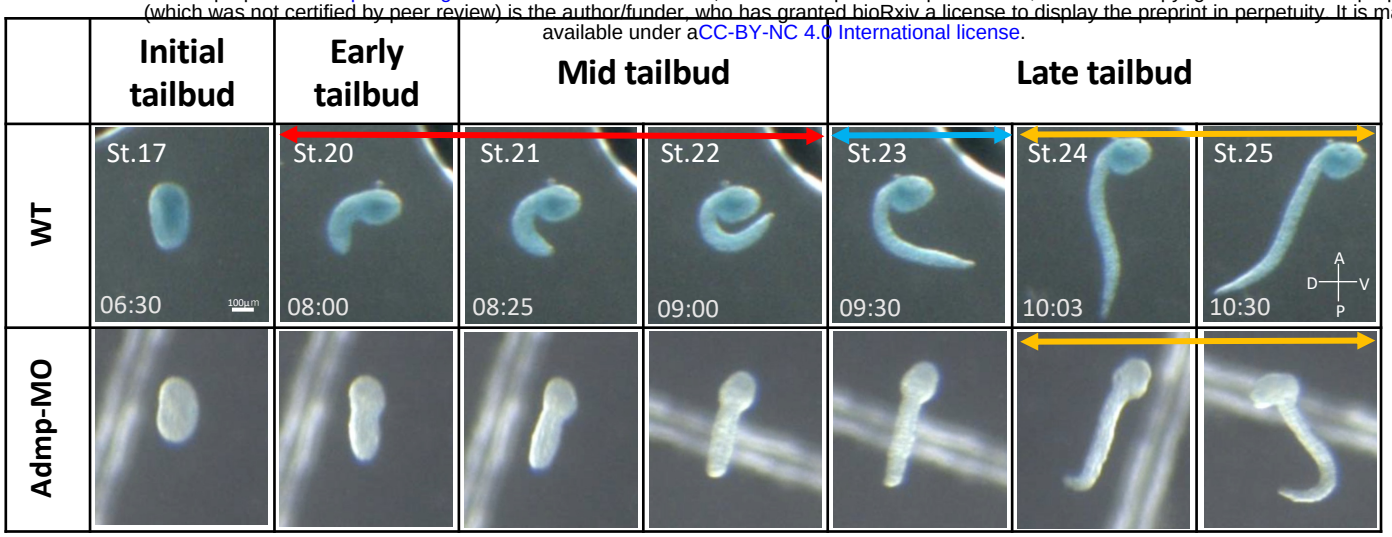


B

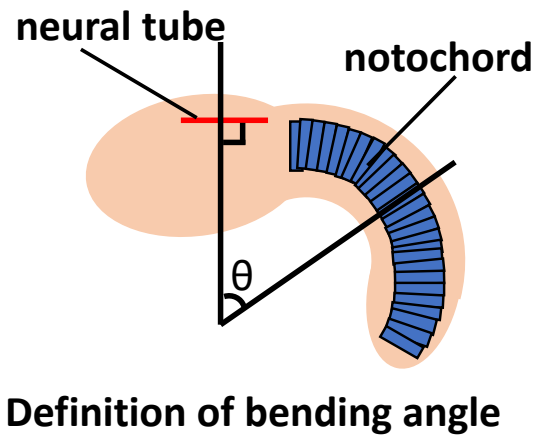


Definition of bending angle

C

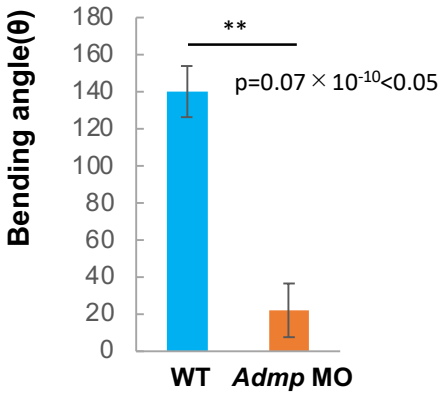


D

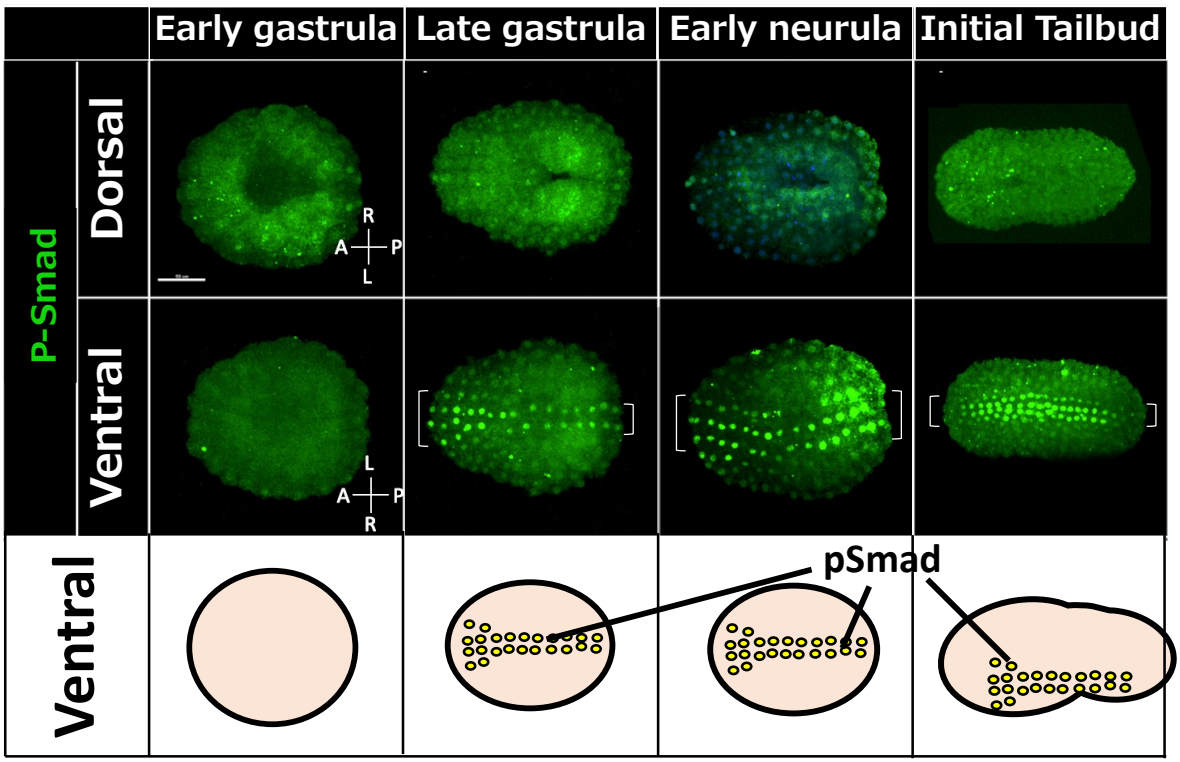


**Fig. 1**

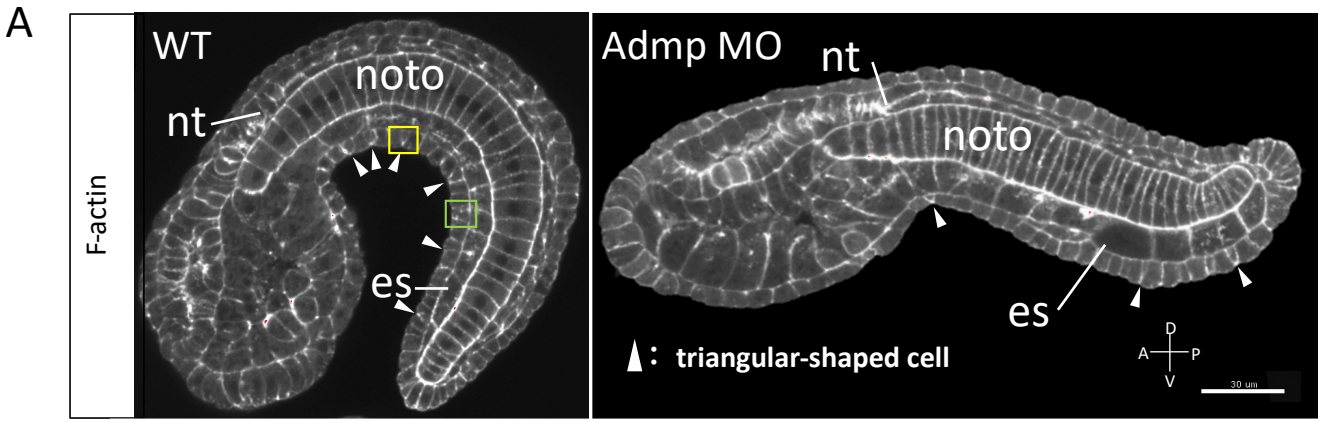


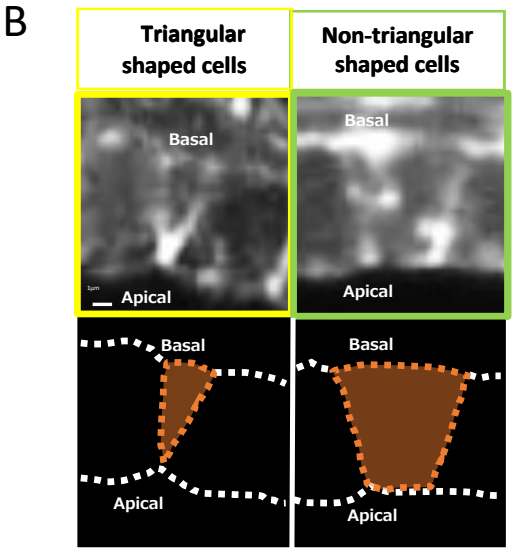


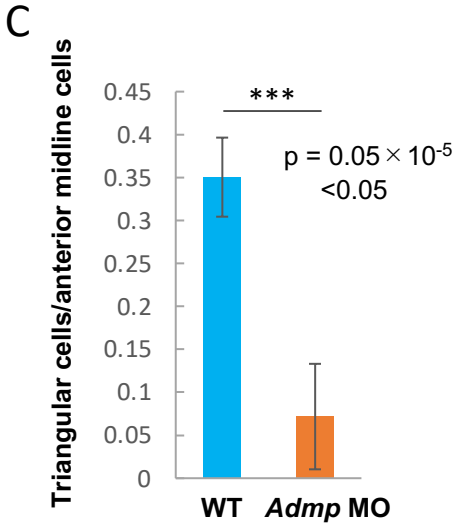


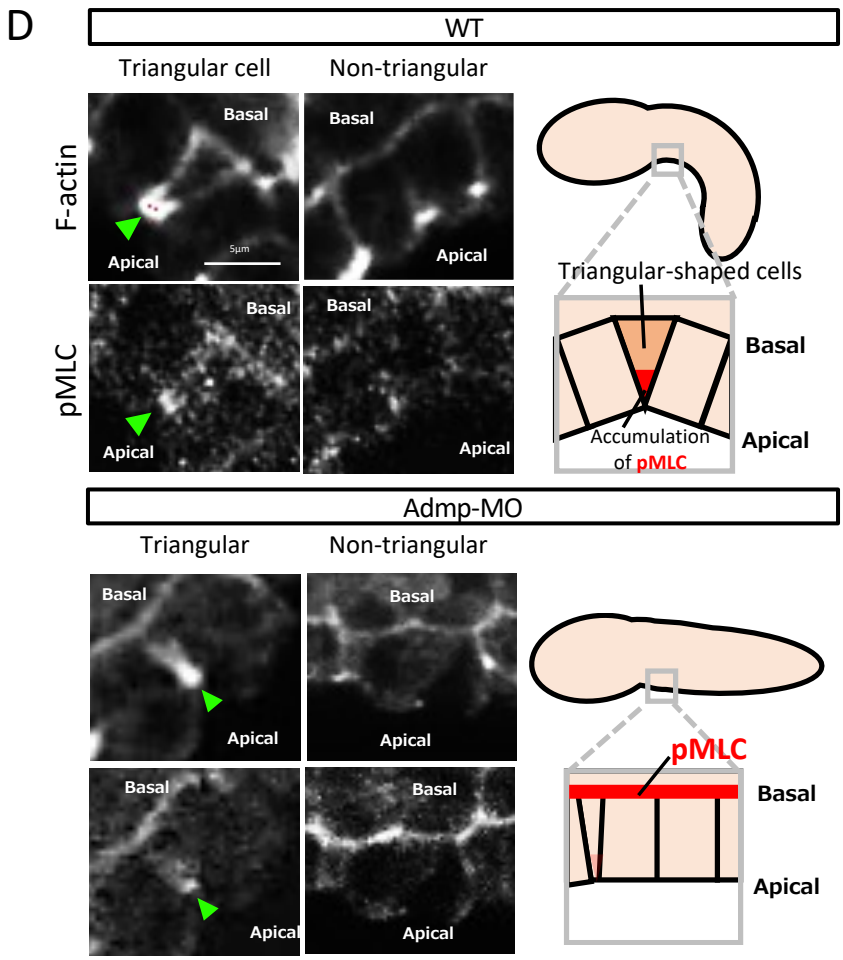


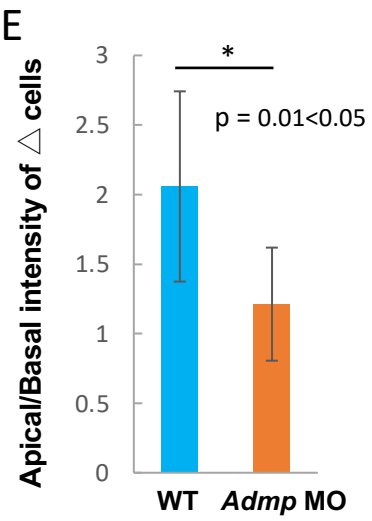


**Fig. 2** ▲ : apical apex of triangular cell

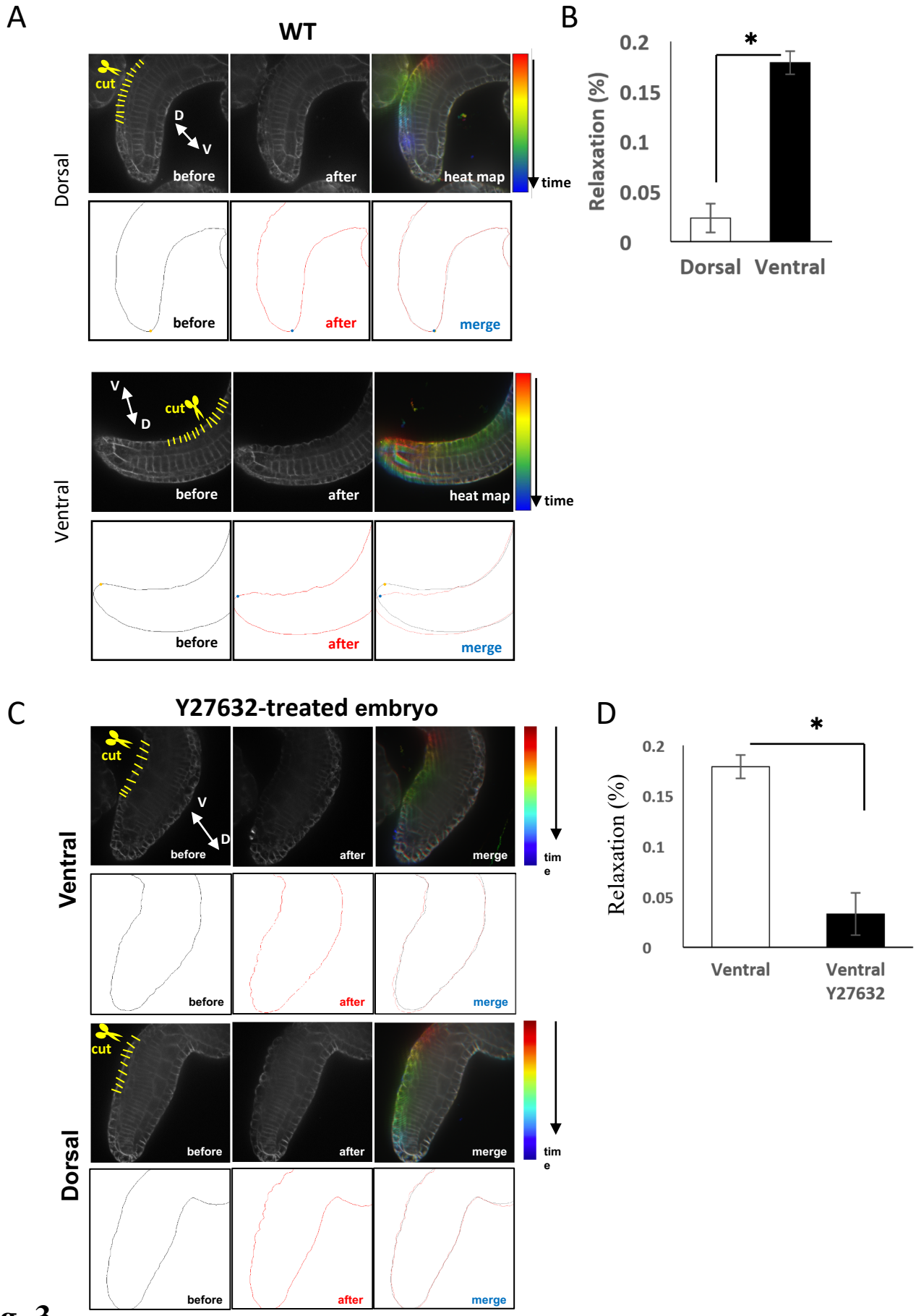
A
WT
Dorsal
cut
D
V
before
after
heat map
time
before
after
merge
Ventral
V
D
cut
before
after
heat map
time
before
after
merge
B
Relaxation (%)
0.2
0.15
0.1
0.05
0
*
Dorsal
Ventral
C
Y27632-treated embryo
Ventral
cut
V
D
before
after
merge
time
before
after
merge
Dorsal
cut
before
after
merge
time
before
after
merge
D
Relaxation (%)
0.2
0.15
0.1
0.05
0
*
Ventral
Ventral
Y27632

**Fig. 3**

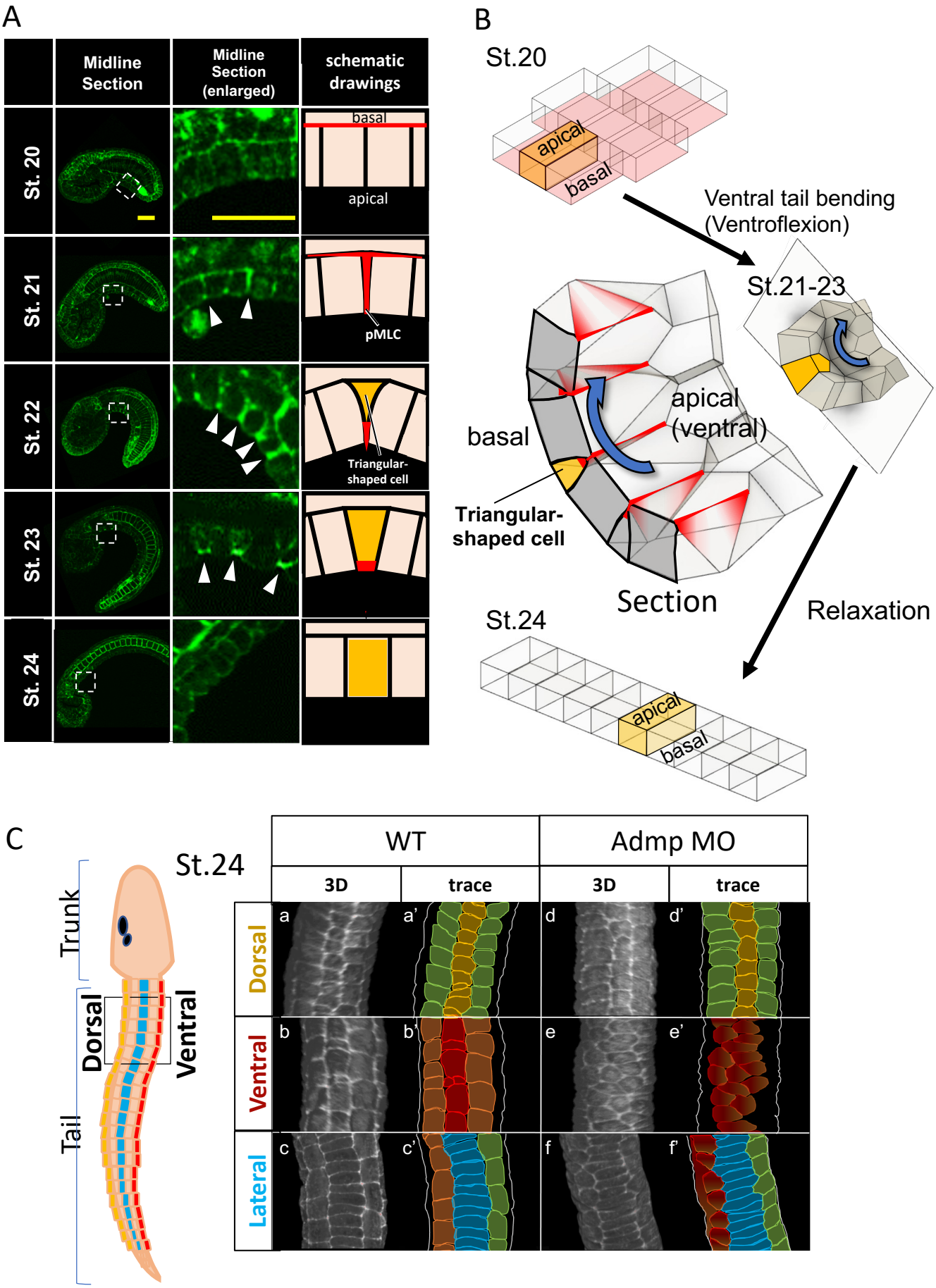
A
Midline Section
Midline Section (enlarged)
schematic drawings
St. 20
St. 21
St. 22
St. 23
St. 24
basal
apical
pMLC
Triangular-shaped cell
B
St.20
apical
basal
Ventral tail bending (Ventroflexion)
St.21-23
apical (ventral)
basal
Triangular-shaped cell
Section
Relaxation
St.24
apical
basal
C
St.24
Trunk
Tail
Dorsal
Ventral
WT
Admp MO
3D
trace
Dorsal
Ventral
Lateral
a
a'
b
b'
c
c'
d
d'
e
e'
f
f'

**Fig. 4**

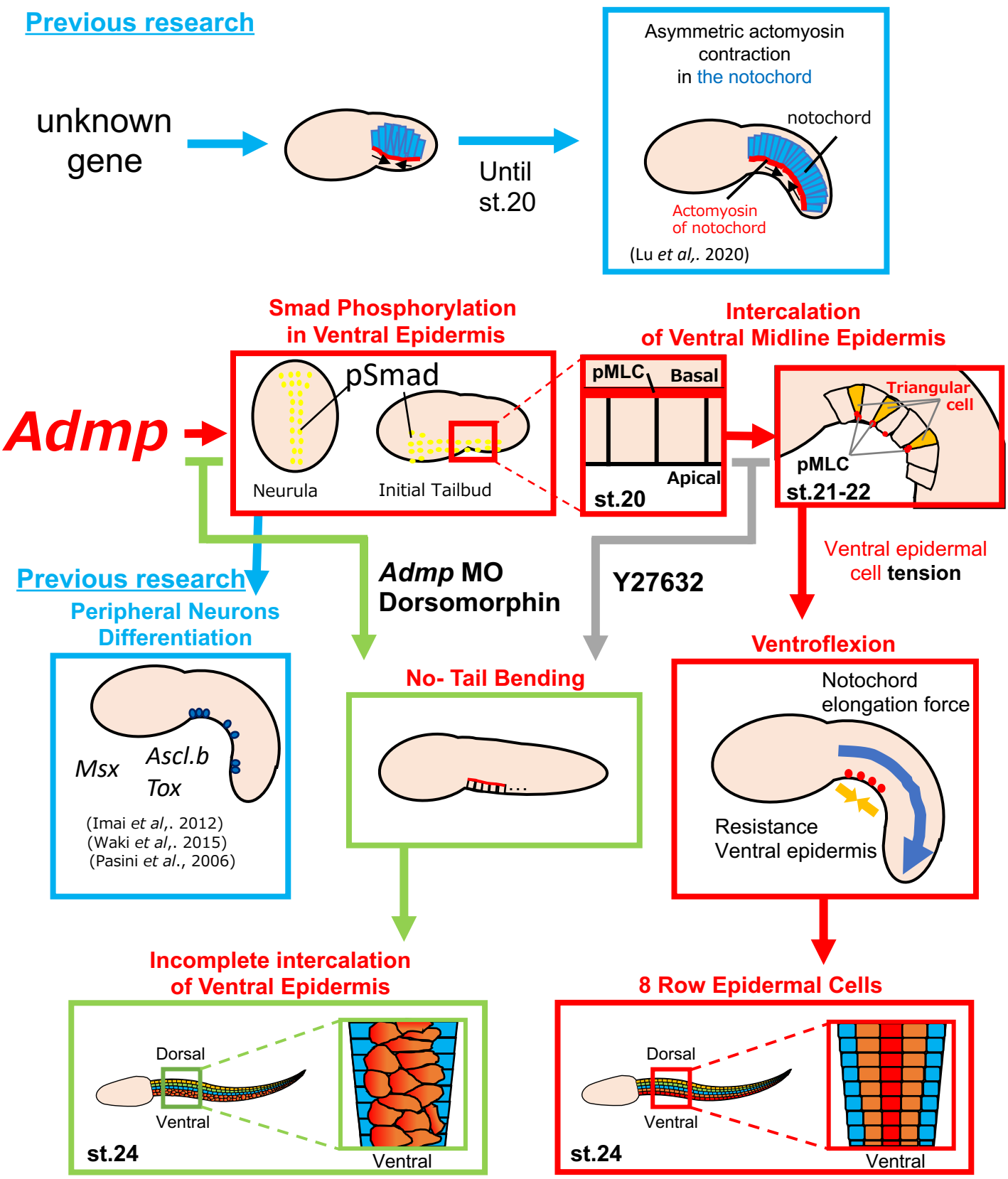
Previous research
unknown gene
Until st.20
Asymmetric actomyosin contraction in the notochord
notochord
Actomyosin of notochord
(Lu et al,. 2020)
Admp
Smad Phosphorylation in Ventral Epidermis
pSmad
Neurula
Initial Tailbud
pMLC
Basal
Apical
st.20
Intercalation of Ventral Midline Epidermis
Triangular cell
pMLC
st.21-22
Ventral epidermal cell tension
Previous research
Peripheral Neurons Differentiation
Msx
Ascl.b
Tox
(Imai et al,. 2012)
(Waki et al,. 2015)
(Pasini et al., 2006)
Admp MO
Dorsomorphin
Y27632
No- Tail Bending
Ventroflexion
Notochord elongation force
Resistance
Ventral epidermis
Incomplete intercalation of Ventral Epidermis
Dorsal
Ventral
st.24
Ventral
8 Row Epidermal Cells
Dorsal
Ventral
st.24
Ventral

**Fig. 5**

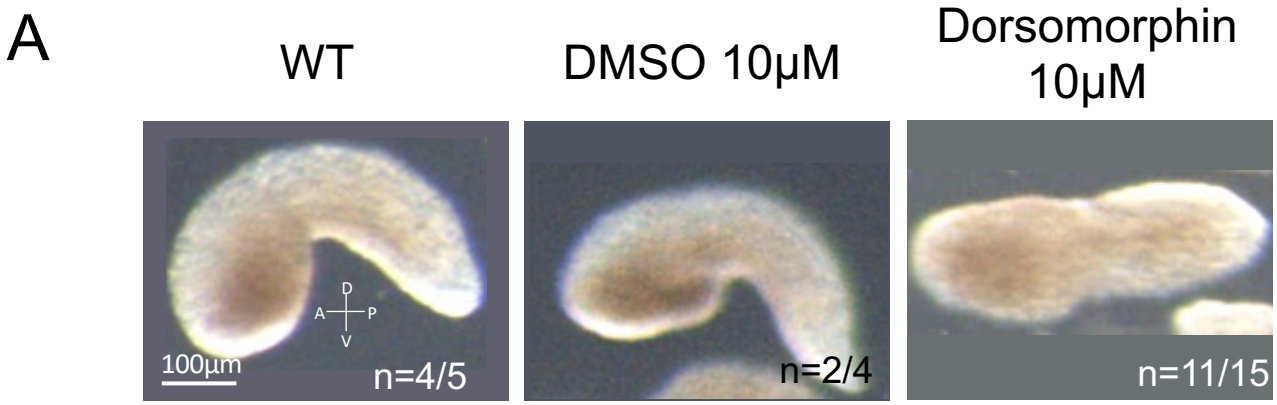
A
WT
DMSO 10µM
Dorsomorphin
10µM
D
A
P
V
100µm
n=4/5
n=2/4
n=11/15

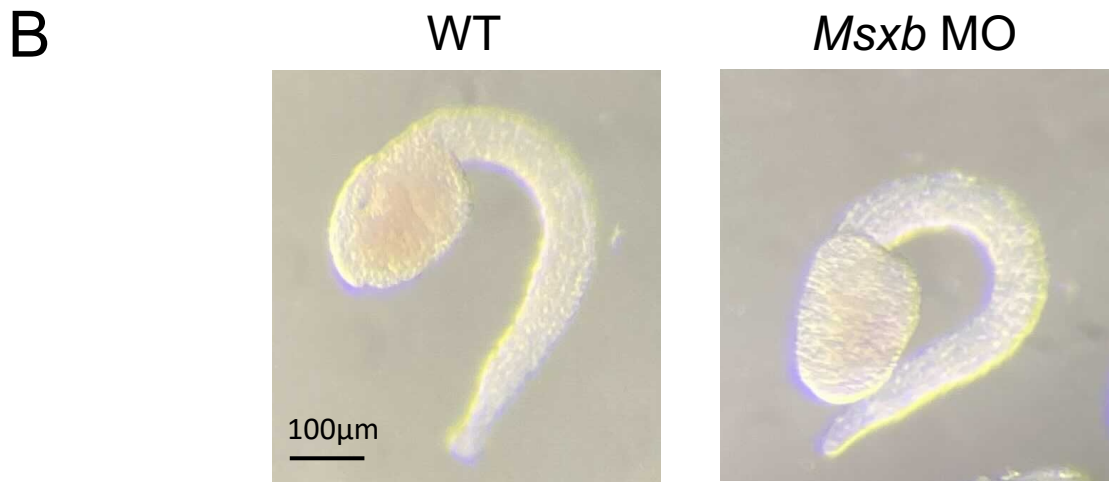
B
WT
*Msxb* MO
100µm

**Suppl.Fig. 1**

**A**

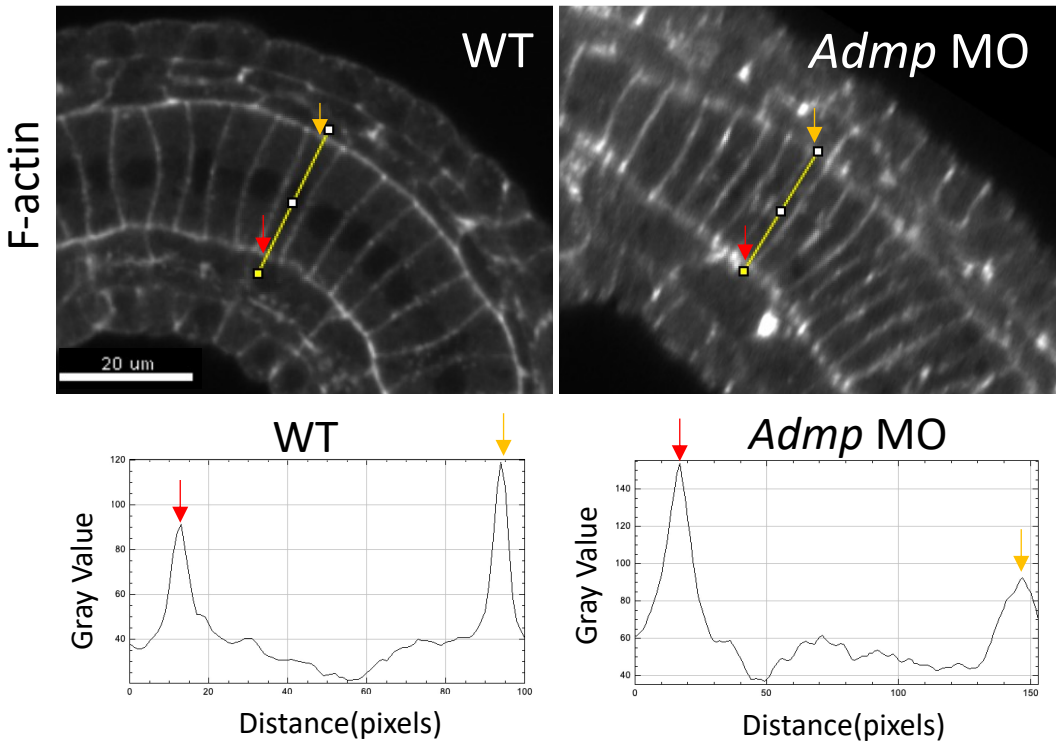


**B**

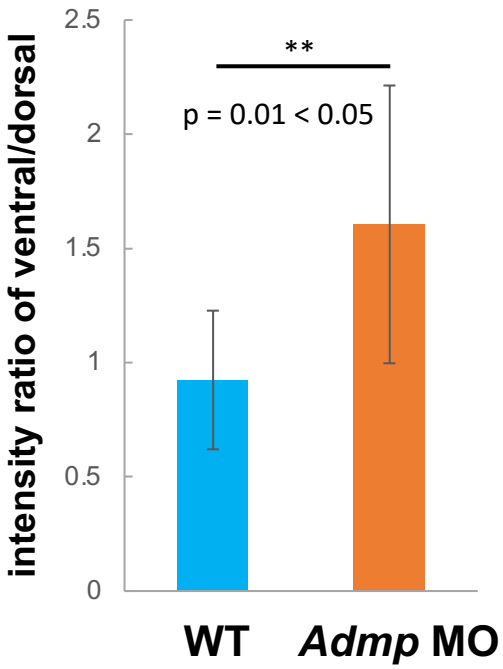


**Suppl.Fig. 2**

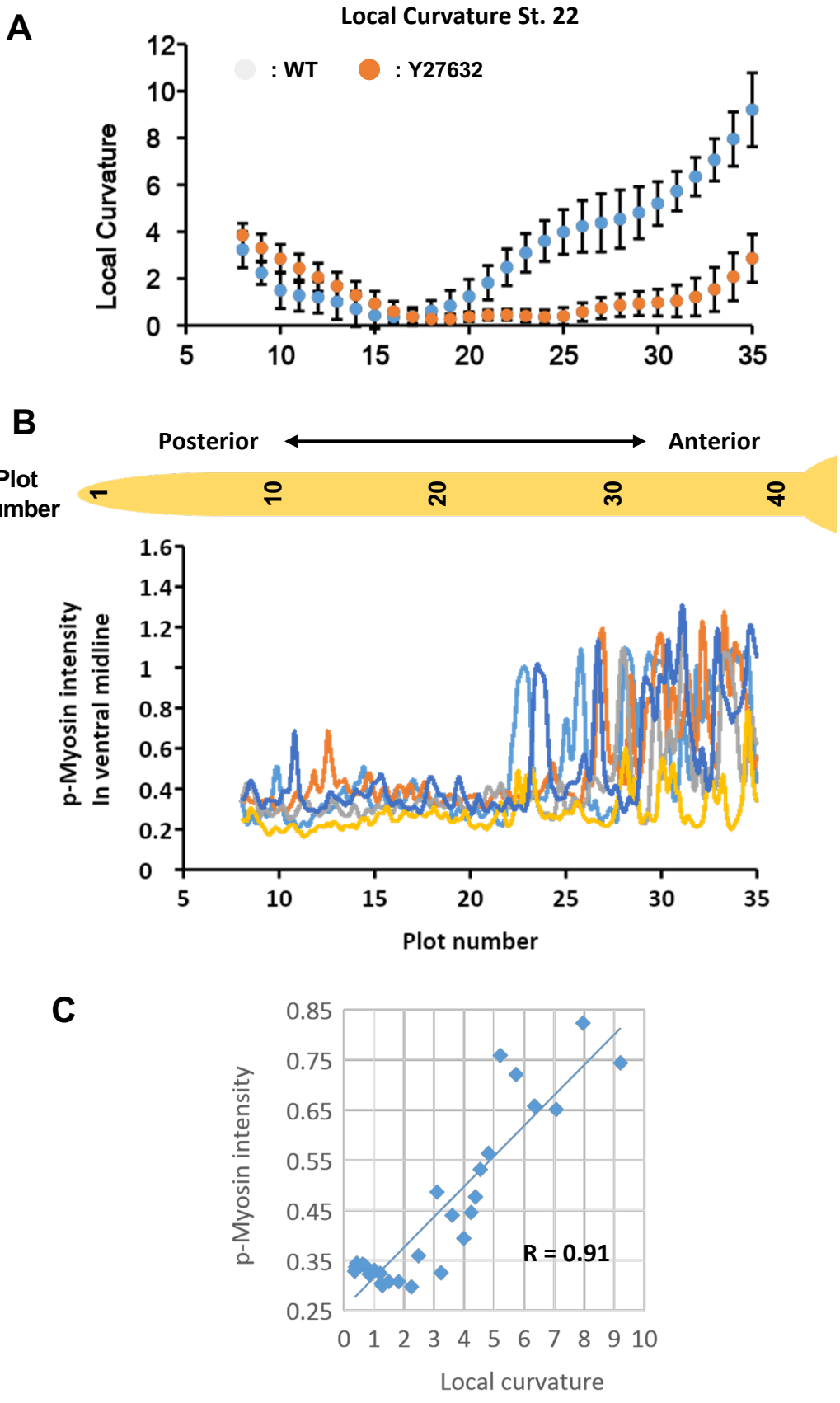
A
Local Curvature St. 22
: WT
: Y27632
Local Curvature
B
Posterior
Anterior
Plot Number
p-Myosin intensity In ventral midline
Plot number
C
p-Myosin intensity
R = 0.91
Local curvature

**Suppl.Fig. 3**

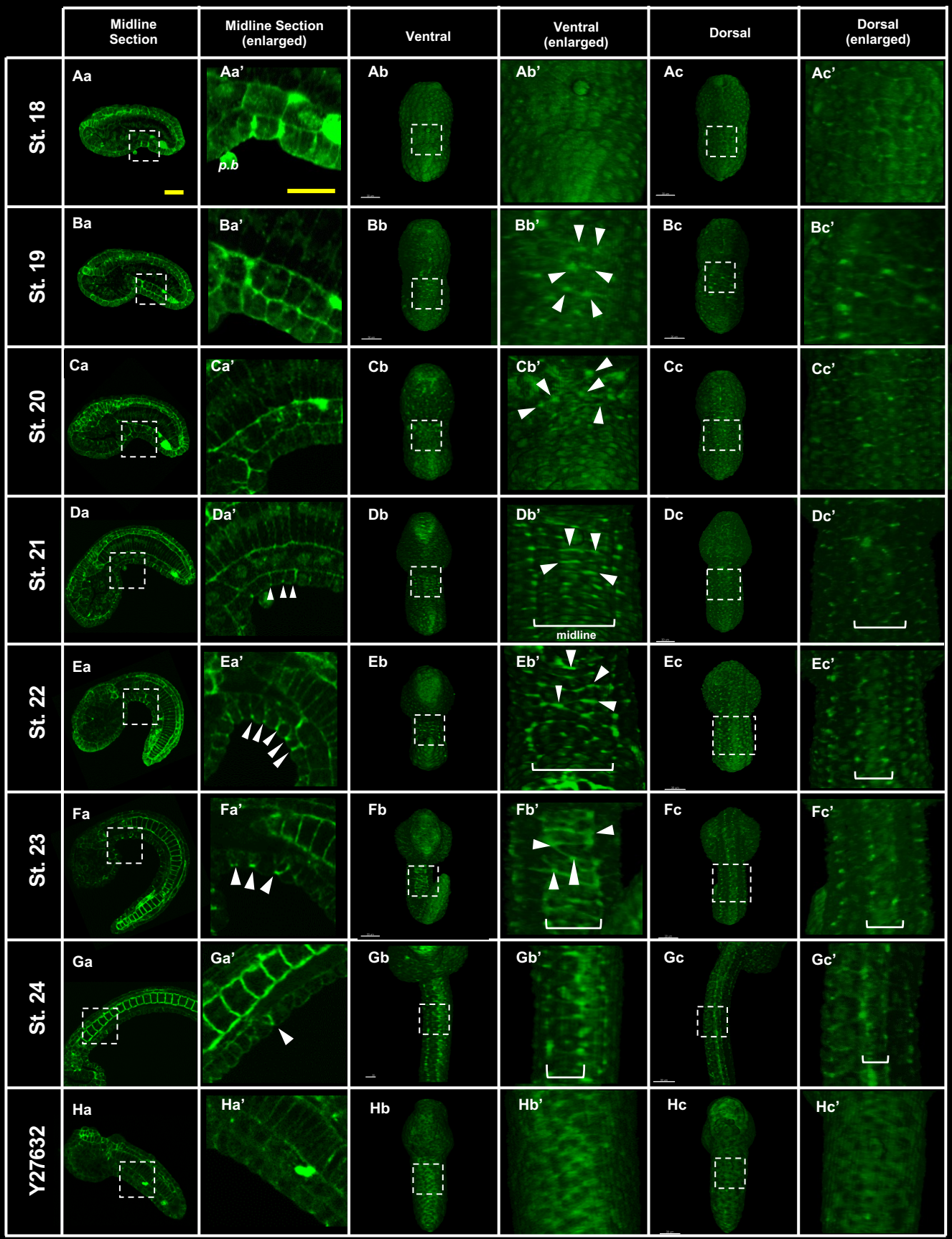
Midline Section
Midline Section (enlarged)
Ventral
Ventral (enlarged)
Dorsal
Dorsal (enlarged)
St. 18
St. 19
St. 20
St. 21
St. 22
St. 23
St. 24
Y27632
Aa
Aa'
Ab
Ab'
Ac
Ac'
p.b
Ba
Ba'
Bb
Bb'
Bc
Bc'
Ca
Ca'
Cb
Cb'
Cc
Cc'
Da
Da'
Db
Db'
Dc
Dc'
midline
Ea
Ea'
Eb
Eb'
Ec
Ec'
Fa
Fa'
Fb
Fb'
Fc
Fc'
Ga
Ga'
Gb
Gb'
Gc
Gc'
Ha
Ha'
Hb
Hb'
Hc
Hc'

**Suppl.Fig. 4**

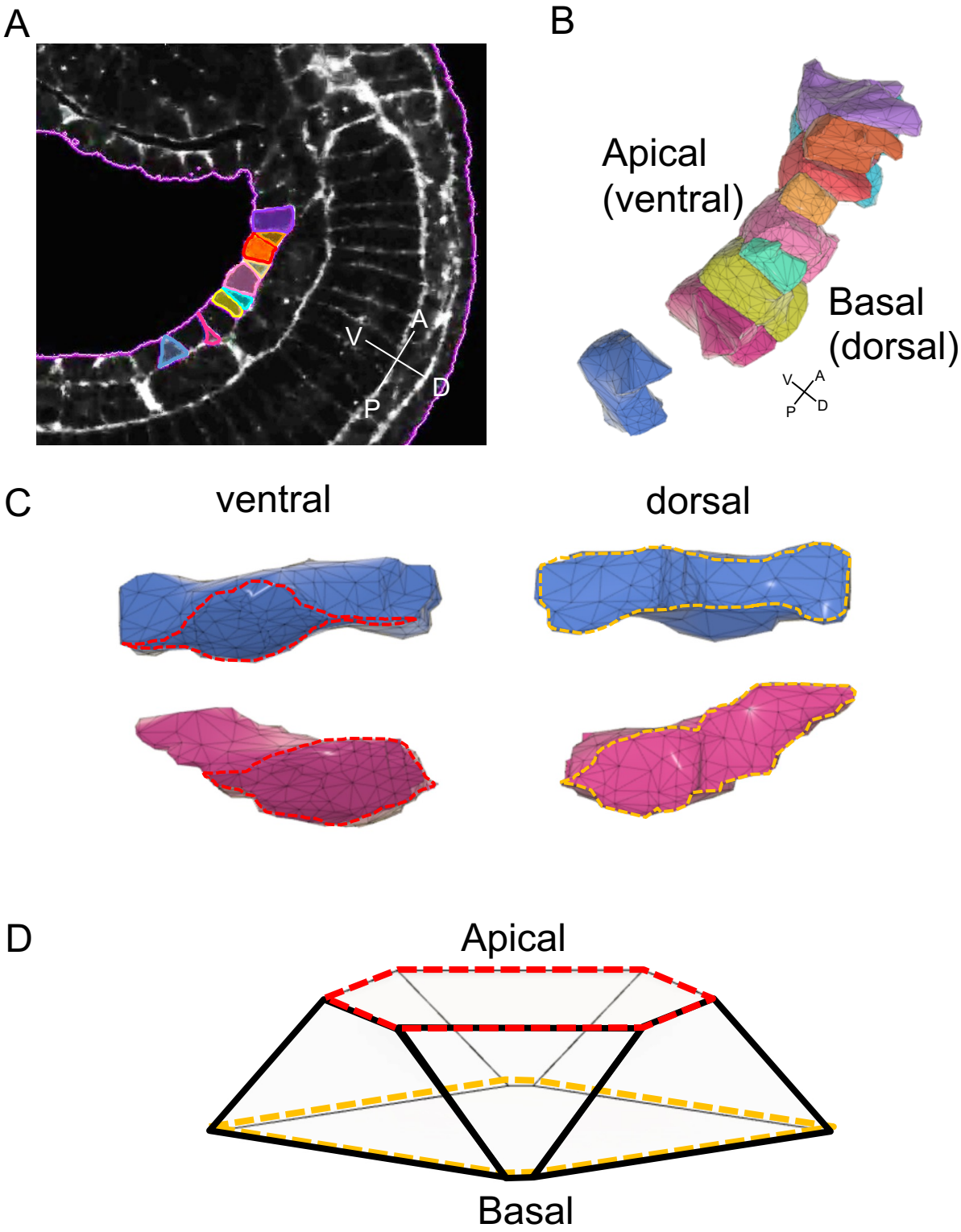
A
V
A
P
D
B
Apical
(ventral)
Basal
(dorsal)
V
A
P
D
C
ventral
dorsal
D
Apical
Basal

**Suppl.Fig. 5**

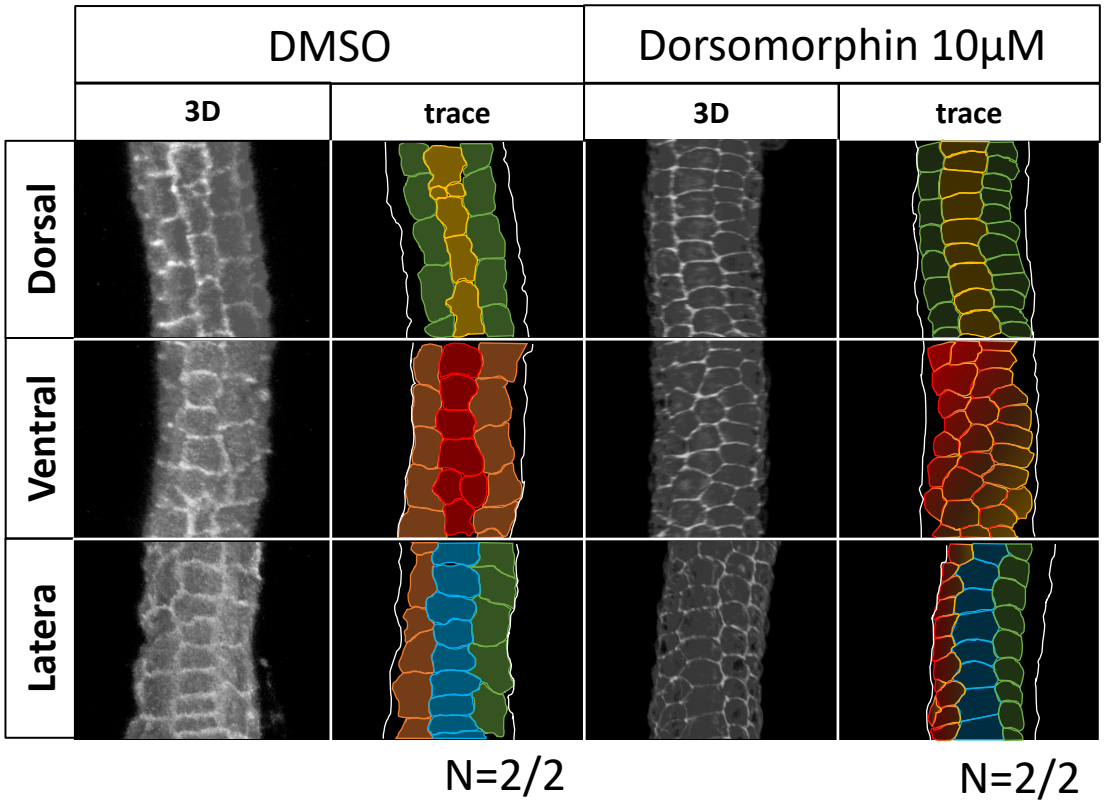
DMSO
Dorsomorphin 10µM
3D
trace
3D
trace
Dorsal
Ventral
Latera
N=2/2
N=2/2

**Suppl.Fig. 6**

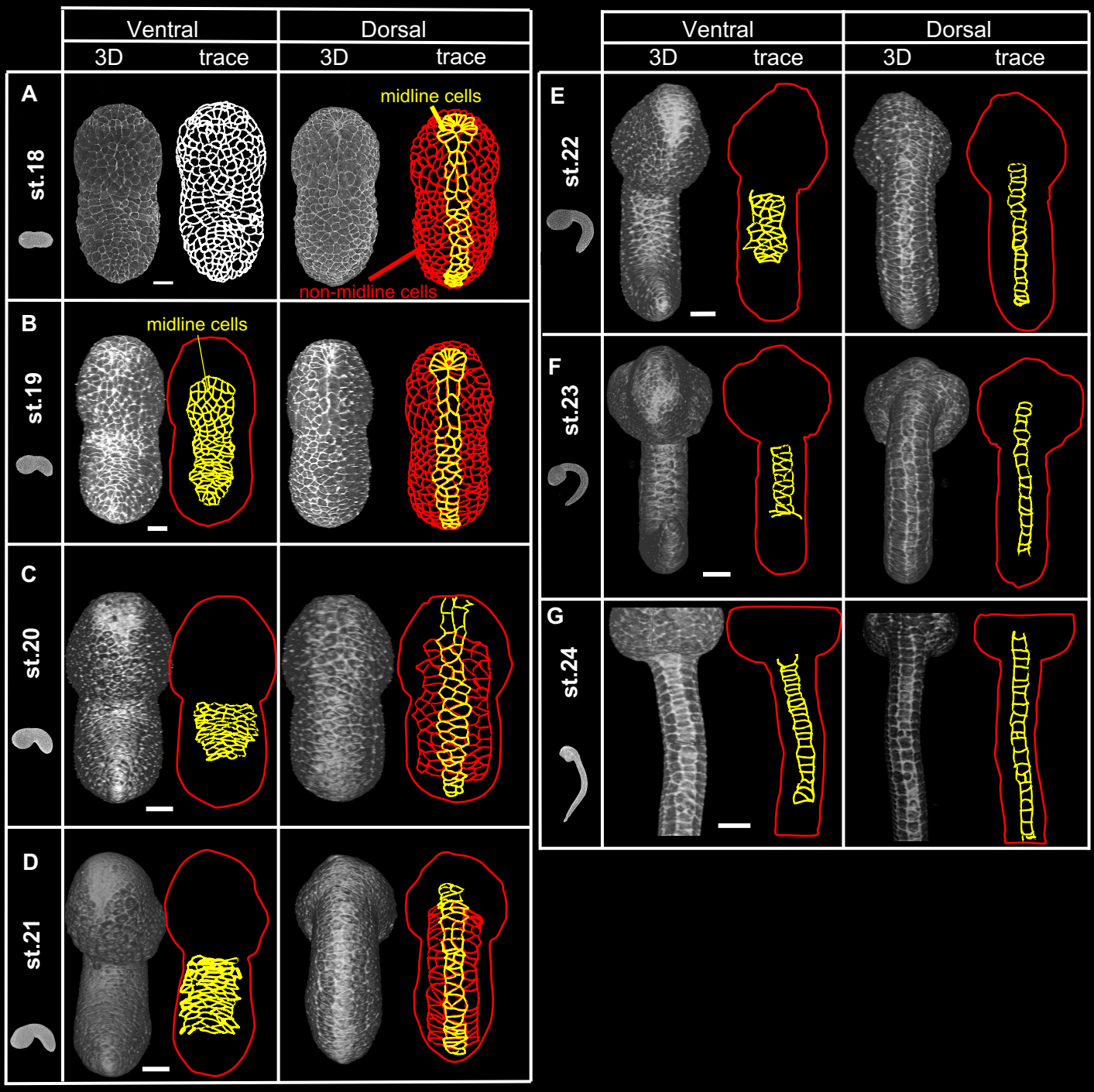
Ventral
Dorsal
3D
trace
3D
trace
A
st.18
midline cells
non-midline cells
B
st.19
midline cells
C
st.20
D
st.21
E
st.22
F
st.23
G
st.24

Suppl.Fig. 7

A

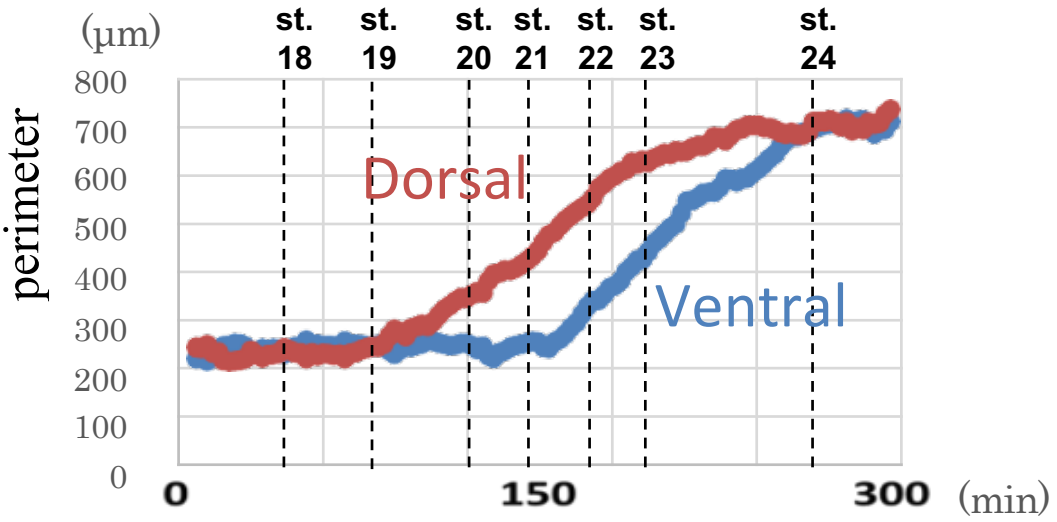


B

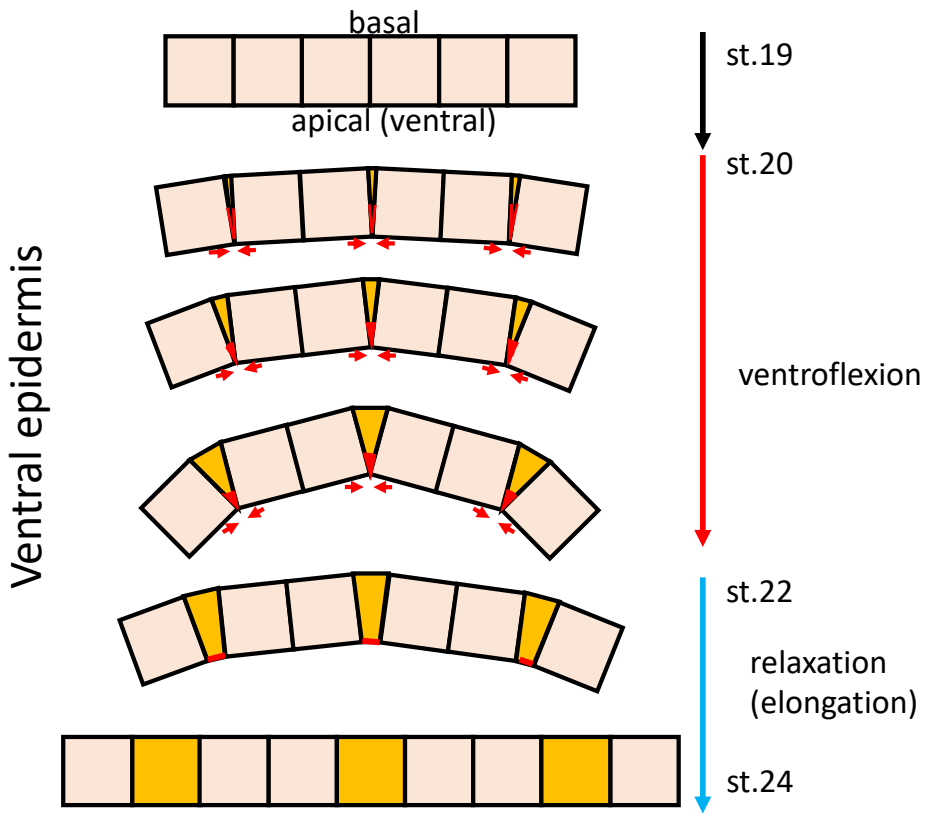


**Suppl.Fig. 8**